Journal of Structural Geology, Vol. 10, No. 7, pp. 649 to 659, 1988
Printed in Great Britain

0191-8141/88 $03.00 + 0.00

How normal faulting and sedimentation interact to produce listric fault profiles and stratigraphic wedges

BRUNO VENDEVILLE* and PETER R. COBBOLD

Laboratoire de Tectonophysique, Institut de Géologie, Université de Rennes, 35042 Rennes Cédex, France

(*Received* 6 *April* 1987; *accepted in revised form* 25 *May* 1988)

Abstract—In a series of scale-experiments, we generated listric normal faults by extending models composed of colored sand layers deposited at regular time intervals throughout deformation during syntectonic sedimentation. Progressive bulk extension along a single set of faults caused domino-type tilting of fault blocks. Underlying tilted faults propagated upwards, with constant dips into newly sedimented layers. Hence fault profiles become progressively more listric. Tilting of the free surface resulted in asymmetrical depressions and in fan-shaped deposits.

Stepwise or continuous geometric models of domino-tilting and synchronous sedimentation yield the same structural and stratigraphic features as observed in the sand models. The continuous geometric model shows that a critical parameter governing fault curvature is the ratio R between rates of bulk strain and sedimentation.

Both types of models reveal that synchronous sedimentation and bulk extension are capable by themselves of generating listric normal faults.

INTRODUCTION

THE origin of the term 'listric' has been discussed in detail by Bally *et al.* (1981): it derives from the Greek 'listron', a shovel. The current usage is mainly geometric. A listric fault has curvature and may be concave or convex upwards. At first, listric faults were mainly described from relatively near-surface sedimentary sequences. In such a context, listric faults commonly flatten into weak stratigraphic layers or detachment horizons at depth (Rettger 1935, Woodbury *et al.* 1973, Bally 1981, Ewing 1983, Gawthorpe & Clemmey 1985). Since then, deeper seismic profiles have suggested that listric normal faults occur at crustal scale, involving basement as well as cover rocks (see, for example, Lowell *et al.* 1975, Guennoc 1978, Eaton 1980, Montadert *et al.* 1979, Le Pichon & Sibuet 1981, Chenet 1983, Beach *et al.* 1987, Gibbs 1987).

There is no consensus as to the mechanisms leading to listric normal faulting. According to mechanical studies (e.g. Hafner 1951, Price 1977, Crans *et al.* 1980) normal faults may initially form with a listric shape. Fault curvature results from vertical changes in (i) principal stress orientations, due essentially to boundary conditions (Hafner 1951, Odé 1960, Price 1977) or (ii) rheology, due, for example, to geothermal gradients, or to fluid overpressure during compaction (Hubbert & Rubey 1959, Bruce 1973, Crans *et al.* 1980, Jackson & McKenzie 1983). Other authors (e.g. Roux 1979, Jones & Addis 1984) suggest that fault curvature may be mainly a secondary feature, acquired or accentuated by the deformation accompanying differential compaction (Carver 1968, Jones & Addis 1984, Shelton 1984) or progressive fault slip (Roux 1979, Shelton 1984). Clearly, different mechanisms are to be expected, according to the tectonic context and especially the depth to which normal faults penetrate.

In this paper, we focus on the well-known context of growth faulting in deltaic environments, where normal faults typically occur up to depths of less than 5 km and cut through poorly consolidated sediments (Cloos 1968, Woodbury *et al.* 1973, Edwards 1976, Weber & Daukoru 1976, Evamy *et al.* 1978, Rider 1978, Ewing 1983, 1984, Garfunkel 1984, Jackson & Galloway 1984, Rouchy 1986). Sedimentation in such environments is usually relatively rapid and more than compensates for the stratigraphic thinning caused by faulting. The dynamic cause of faulting in growth-faulted terranes is usually assumed to be gravitational gliding down delta slopes (Terzaghi 1956, Crans *et al.* 1980, Mandl & Crans 1981, Erxleben & Carnahan 1983, Garfunkel 1984, Rouchy 1986). In this paper we concentrate not on dynamic causes of faulting but on the mechanism responsible for fault curvature. In particular, we investigate the effect of progressive sedimentation during deformation, since such a condition is, by definition, necessary for growth faults.

Our approach utilized two methods. First, we built scale models made essentially of sand and subjected them to horizontal extension and vertical shortening during ongoing stepwise sedimentation. Second, we extracted the main features observed in the scale models and used them to make simple geometrical models.

SAND MODELS OF DOMINO-SEDIMENTATION

Principles

All the experiments were conducted in the Experimental Tectonics laboratory at the University of

*Present address: Center for Tectonophysics, College of Geosciences, Texas A & M University, College Station, TX 77843, U.S.A.

Rennes. Construction of any experimental as well as analytical models requires some assumptions and simplifications on the kinematics and the mechanics of the natural example. First, in the following approach we consider that extension is uniform at the base of the system. Although data in growth faulted terranes suggest that the horizontal stretching is not strictly uniform at the base of the faulted sequence, construction of models with a uniform extension is a necessary condition to allow a detailed geometric analysis of the domino-sedimentation process. Second, we constructed models which simulate brittle sedimentary rocks, assumed to deform by motion along discrete fault planes or narrow shear zones. We also assume that initial fault orientation is controlled by the stress field only, and that fault planes also are major planes of weakness allowing large rotations of fault blocks.

For technical reasons, the scale factor for length between the models and their idealized natural counterpart was 10^5 (1 cm in experiment represents 1 km in nature). The application of the principles of scaling analysis defined by Hubbert (1937) and Ramberg (1967) requires the use of an analogue material which has a rheological behavior similar to the natural examples and which is 10^5 times weaker than natural rocks.

For scale factors between 10^4 and 10^7, dry sand has been found to be a convenient analogue for brittle rocks in numerous previous experimental studies (Hubbert 1951, Horsfield 1977, Faugère & Brun 1984, Brun *et al.* 1985, Naylor *et al.* 1986, Vendeville & Cobbold 1987, Vendeville *et al.* 1987).

Uncompacted dry sand deforms essentially by faulting. Fault planes form by local dilatancy of the sand pack along discrete fault planes or narrow shear zones (Mandl *et al.* 1977). This is accompanied by a significant softening along the fault plane (see Mandl *et al.* 1977, fig. 8). Hence, once formed the fault planes represent planes of low resistive shear strength on which motion will preferentially occur during subsequent deformation stages unless no kinematic conditions preclude block motion.

Fault-plane orientation in dry sand mostly depends on the orientation of the applied stress field. Dry sand typically obeys a Mohr–Coulomb criterion of failure:

$$\tau = C_o + \sigma_n \tan \phi,$$

where σ_n and τ are, respectively, the normal and shear stresses acting on the fault plane, C_o is the cohesion and ϕ the friction angle. Since the value of the friction angle (about 30–31°) is identical in nature and sand, the rheological behavior can be considered as similar. As shown by Horsfield (1977) and Vendeville (1987), the cohesion in sand models may be a little too small, but its effect becomes rapidly negligible at model depths exceeding 1 cm (representing 1 km). Wet sand, in contrast, has too large a cohesion.

Dry sand behavior can differ to some extent when specific kinematic conditions are applied to the system. First, if boundary conditions imply a bulk regime of simple shear, faults or shear zones develop parallel to the shear plane (Mandl & Fernandez Luque 1970, Mandl *et al.* 1977). Hence they correspond not to Mohr–Coulomb slip planes but are planes of maximum shear strain. Since our models of extension admit at least one free boundary (the top surface), no bulk shear strain can be kinematically imposed and thus fault planes will obey a Mohr–Coulomb criterion.

Second, undeflectable boundaries can preclude discontinuous deformation of the sand. Near such boundaries, sand deforms continuously by internal strain or folding within fault-blocks and formation of thick shear zones. In sand models of extension, this effect mainly occurs near the model base and affects only the lower centimeter of the sand pack (Vendeville *et al.* 1987). In contrast, in mid- and upper-levels, the model deforms along fault planes and blocks remain quasi-rigid. Hence, dry sand models provide the three following characteristics we require to simulate the interaction between faulting, sedimentation and block rotation:

(1) the initial fault orientation depends on the orientation of the stress field only;
(2) once formed, faults are planes of preferential motion. During subsequent stages of deformation they will remain active even for large amounts of block rotation;
(3) they also can propagate upwards into the newly deposited layers during sedimentation synchronous with faulting.

From a technical point of view, dry sand also has many advantages over other analogue material (e.g. clay) for modeling synsedimentary processes (see Horsfield 1977, Vendeville 1987, Vendeville & Cobbold 1987). It allows rapid sequential sedimentation—uniform or non-uniform—of an homogeneous layer with rheological properties identical to those of the lower layers.

For all these reasons, we used a natural quartz sand from Fontainebleau, with well-rounded grains. The sand was sieved to obtain a grain size of 200–300 μm and then we colored various batches using organic or mineral pigments.

Construction and deformation

We built and deformed the models in a single rectangular sandbox, 10 cm deep, 20 cm long and 25 cm wide (to avoid excessive boundary friction during deformation). Models were built by dry sedimentation of several discrete layers, a few mm thick, with contrasting colors. Each layer was poured by hand, from a beaker moved along the model a few cm above its free upper surface.

After or during sedimentation the models were allowed to stretch in one horizontal direction. This was done by displacing one of the piston-like endwalls at a steady rate, using a screw-jack driven by a stepping motor with a computer control. We obtained uniform extension at the base of each model by stretching a latex rubber sheet (as in Vendeville *et al.* 1987). In some models (model 2, Fig. 3) we placed a thin layer of silicone putty at the base, to simulate a ductile horizon of

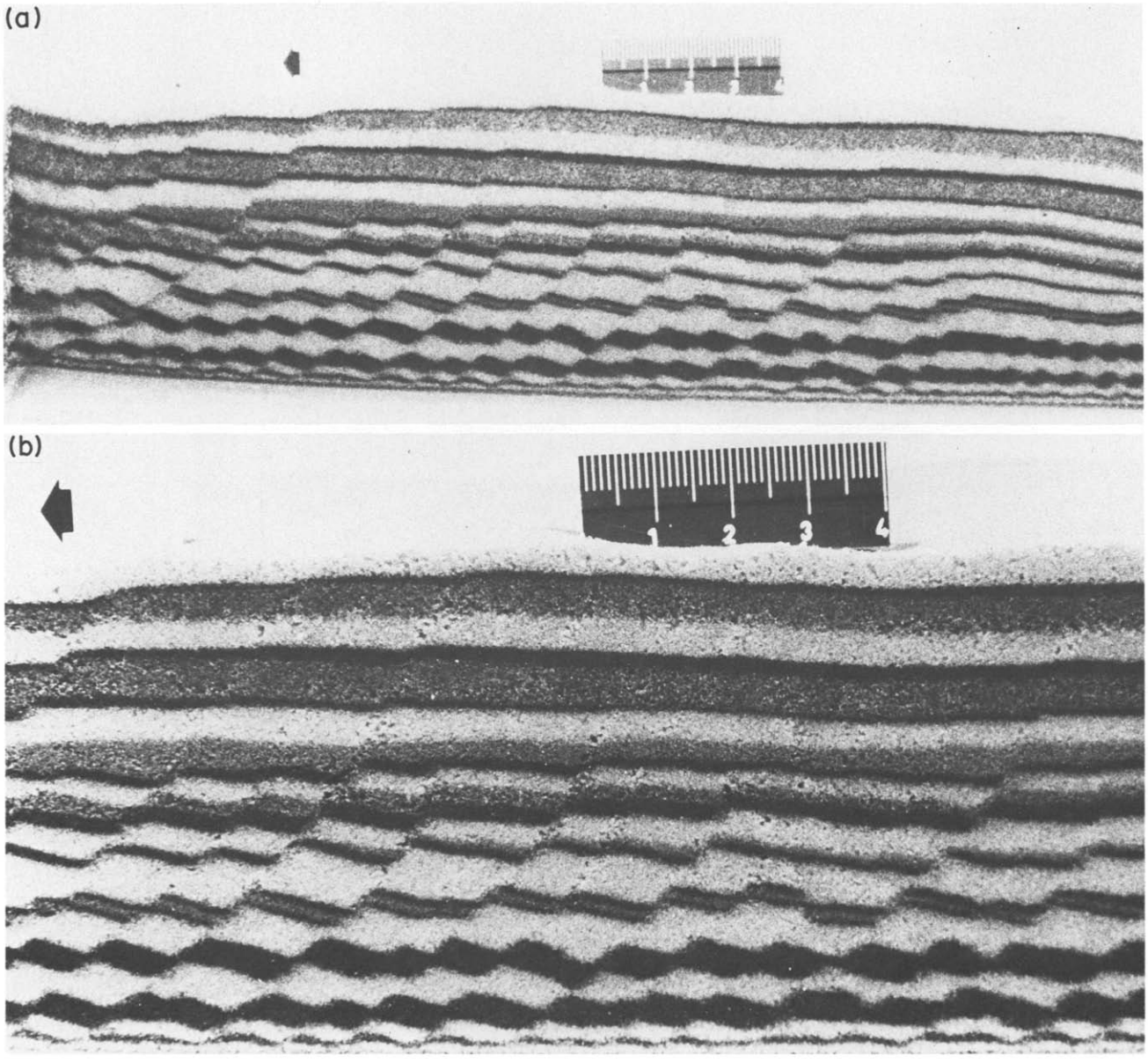

Fig. 1. (a) Longitudinal section through sand model 1. Width of model normal to section was 25 cm; initial length, 20.8 cm; initial thickness, 3 cm; final length, 33.4 cm (61% extension); basal slope, 7°; sedimentation every 15% extension. (b) Close-up of same, showing details of bedding and fault geometry.

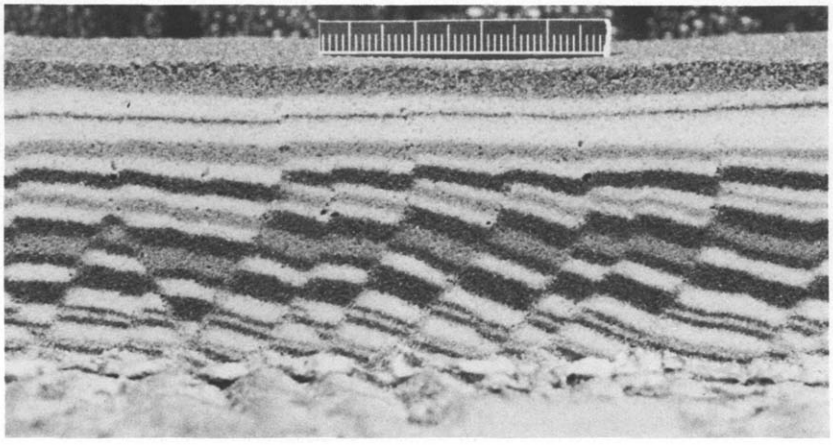

Fig. 2. Longitudinal section through sand model 2. Initial thickness was 2 cm, resting on 0.5 cm of silicone putty; initial length, 29 cm; final length, 41.5 cm (43% extension); basal slope, 7°; sedimentation every 5% extension; piston velocity, 14 cm h^{-1}.

shales or evaporites. Ductile deformation of the silicone layer accommodated, at depth, large displacements along fault planes in the overlying brittle layers and allowed rotation of fault blocks without any significant problem with gaps at the base of the sand layer.

Deformation of the models produced normal faults, inclined at about ±30° to the vertical. These are the two conjugate orientations predicted by Mohr–Coulomb theory, following the assumption that the maximum principal compressive stress was vertical. When the base of the sandbox was kept horizontal during deformation, equal numbers of both conjugate sets of normal faults appeared. When the base was inclined at 3–9° to the horizontal, only one set formed, dipping downslope (Vendeville *et al.* 1987). We used the inclined models, because they resulted in large domino-style rotations of fault blocks.

The initial model thickness, before deformation, was 2–3 cm. After 5–15% extension, fault traces separating asymmetric depression with tilted bottoms were clearly visible at the free surface. Another sand layer was then deposited. Increments of sedimentation were thus repeated, stepwise, until the models were 5–6 cm thick and total extensions were 40–70%. At each step, photographs were taken of the free upper surface.

After deformation, the models were sprayed with water until saturated in order to increase the cohesion, and serially sectioned and photographed. Fault geometries from top views and from vertical sections varied little across model widths, except near the sidewalls. Profile views of faults through the sidewall were not representative of fault geometries in the central part of the models. This result we attribute to sidewall friction (Vendeville *et al.* 1987). Hence, we obtained true profiles only for the final states. This drawback was to some extent offset by repeating the experiments and stopping them, at various stages. This procedure also showed the experiments to be broadly reproducible, although in detail no two fault patterns were ever strictly identical.

Results

Final longitudinal profiles (Figs. 1 and 2) show the following general features.

(1) Most faults are listric (concave upwards). At the free surface, fault dips are about 60° (with respect to the horizontal during deformation); at depth, they are as low as 30°. Fault curvature decreases a little with depth.

(2) Most faults dip downslope.

(3) The width of fault blocks and the horizontal spacing between faults increase upwards, in two different ways. First, the length of bed segments between adjacent fault planes progressively increases upwards, as a result of progressive domino-type extension and sedimentation. Second, there are more faults at the base of the model than at the top. Many basal faults terminate at intermediate depths, or continue upwards as narrow zones of dilation, without visible offset of bedding.

(4) Bedding at the free surface is nearly parallel to the model base, while bed segments between faults show tilts that increase progressively downwards, reaching values of up to 30°. Offsets across faults increase correspondingly to values of as much as 5 mm (representing 500 m in nature). The angle between bedding and faults is roughly preserved. Near the undeflectable base however, these effects die out to be replaced by more distributed deformation.

(5) Bed segments are not of uniform thickness. They wedge out towards the footwalls of faults and become thicker towards the hanging walls. Interfaces between bed segments are nevertheless nearly planar.

Time-lapse photography of the free upper surface (not illustrated) reveals the following additional features.

(1) Some faults can be tracked throughout the entire model history as they propagate upwards and intersect the free surface. The horizontal distance between neighboring fault traces increases progressively with time.

(2) Certain faults become suddenly inactive and produce no further surface traces.

(3) The free surface becomes tilted between fault traces, producing half-grabens. Intermittent sedimentation re-establishes a more uniform planar surface.

Interpretation

From these observations, we infer the following interpretation of the history of faulting and sedimentation in the models and how these processes interact.

(1) Initial faults are closely spaced, in proportion to the initial stratigraphic thickness (Vendeville *et al.* 1987).

(2) Initial faults propagate upward at about 60° to the horizontal, into newly sedimented layers.

(3) As stratigraphic thickness increases, fault spacing increases in proportion, as previously described for sand models by Vendeville (1987) and Vendeville *et al.* (1987), and visible on some seismic sections in growth-faulted terranes (e.g. Petrobras 1983a & b, Vendeville 1987). Hence some faults become inactive. As a very rough rule, we observed that half of the faults become inactive as stratigraphic thickness doubles.

(4) Except near the model base, finite deformation accumulates by progressive tilting of fault blocks, in almost rigid domino fashion as defined by Proffett (1977), Le Pichon & Sibuet (1981), Wernicke & Burchfiel (1982), Angelier & Colletta (1983) and Brun & Choukroune (1983). Rigidity is demonstrated by conservation of the angle between faults and bedding. This mechanism has been described before in sand models undergoing horizontal extension without synchronous sedimentation (Faugère & Brun 1984, Brun *et al.* 1985, Vendeville 1987, Vendeville *et al.* 1987). In such models, faults are planar or slightly curved and rotate during ongoing extension.

(5) In the present models, synchronous extension and sedimentation generate listric fault profiles. The mechanism is simple. Older beds accumulate more

deformation than younger beds. Therefore, at any given moment, the amount of finite extension increases downwards, from a minimum at the free surface, to a maximum at the base. Because fault tilt increases with deformation, it too must increase downwards. Hence faults flatten with depth.

(6) At the free surface tilting of fault-blocks produces asymmetric depressions. Because the depressions have sloping bottoms, sedimentation results in stratigraphic wedges (Delfaud 1977, p. 208, Boillot *et al.* 1984, p. 100, Anadon *et al.* 1985).

(7) The horizontal spacing of faults at the free surface increases with the cosine of the angle of tilt; but new layeres are deposited horizontally. Hence newer layers are longer than older ones. The segments become buried and so, in any one profile, bed length progressively increases upwards.

(8) For a domino mechanism to operate without causing gaps and overlaps between rigid fault blocks, fault curvature must be invariant along fault planes. In the models, fault curvature tends to decrease with depth. In particular, it decreases suddenly at the stratigraphic level which was the free surface before that deformation increment started. We infer that continual fault slip was accompanied by some ductile strain (or invisible small-scale faulting) within fault blocks. Possibly block boundaries bent slightly to accommodate changes in curvature.

GEOMETRIC MODELS OF DOMINO-SEDIMENTATION

We have incorporated the essential processes inferred from the sand models into simplified geometric models, where sedimentation and deformation accumulate either stepwise or continuously.

Stepwise sedimentation and deformation

We assume an initial thickness of horizontal sediments, cut by one family of evenly spaced normal faults which all dip at about 60° to the bedding (Fig. 3a). An increment of bulk deformation accumulates by rigid tilting of fault blocks of domino type (Fig. 3b). Deposition of a new layer of sediments fills the surface depressions and re-establishes a horizontal free surface (Fig. 3c). Faults then propagate upwards with 60° dips and a new cycle of deformation and sedimentation is imposed (Fig. 3d). We devised a computer algorithm to repeat this simple stepwise procedure over several cycles. We plot the resulting fault and bedding profiles for three stages of finite extension (30, 60 and 100%) and three relative rates of sedimentation and strain (Fig. 4). The rate of sedimentation is expressed as number of beds, 1 unit thick, per 10% of bulk extension (Fig. 4). Initial fault spacing is 10 units in all diagrams. For simplicity, no faults are rendered inactive, although such an additional process is easy to program.

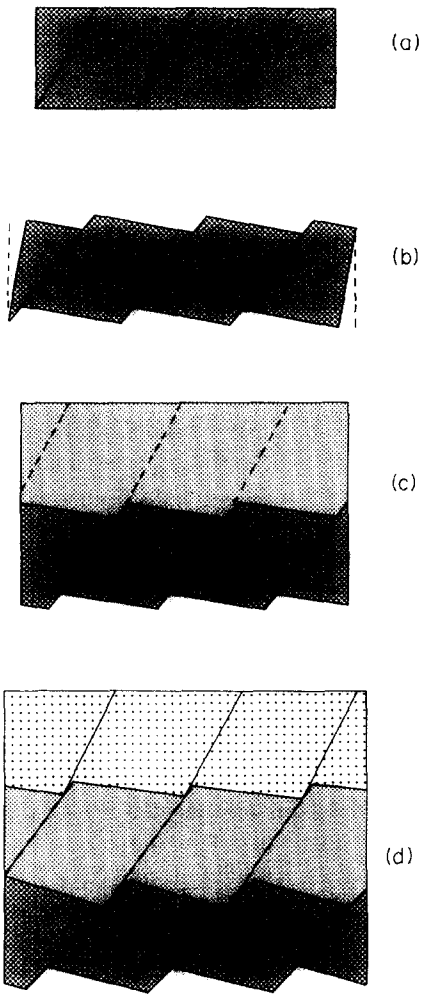

Fig. 3. Four steps illustrating the geometric model of stepwise sedimentation. See text for details.

Continuous sedimentation and deformation

Let z be current depth, measured positively downwards from an origin at the free surface (Fig. 5). An element of current depth, dz, is thus the deformed equivalent of an original material element, dZ, deposited upon the free surface (Fig. 5). The ratio of the two elements is the vertical stretch, $\lambda = \partial z/\partial Z$ (Truesdell & Toupin 1960). In our models, $0 < \lambda < 1$, because there are vertical contractions. The logarithmic stretch is $\varepsilon = \ln \lambda$ which is a negative quantity in the models. The rate of sedimentation with time t is the positive quantity $S = \partial Z/\partial t$. The vertical velocity of a material particle is the negative quantity $\dot{z} = \partial z/\partial t$, where Z is held constant during this operation. The vertical stretching rate (strain rate) is a velocity gradient (Truesdell and Toupin 1960):

$$\dot{\varepsilon} = \partial \varepsilon/\partial t = \partial \dot{z}/\partial z = \dot{\lambda}/\lambda. \quad (1)$$

Hence $\dot{\varepsilon}$ is a negative quantity.

Let us compare the rates of sedimentation and strain, using the ratio $R = \dot{\varepsilon}/S$ (a negative quantity). From the above definitions, we obtain:

$$R = \dot{\varepsilon}/S = \partial \varepsilon/\partial Z = \partial \lambda/\partial z. \quad (2)$$

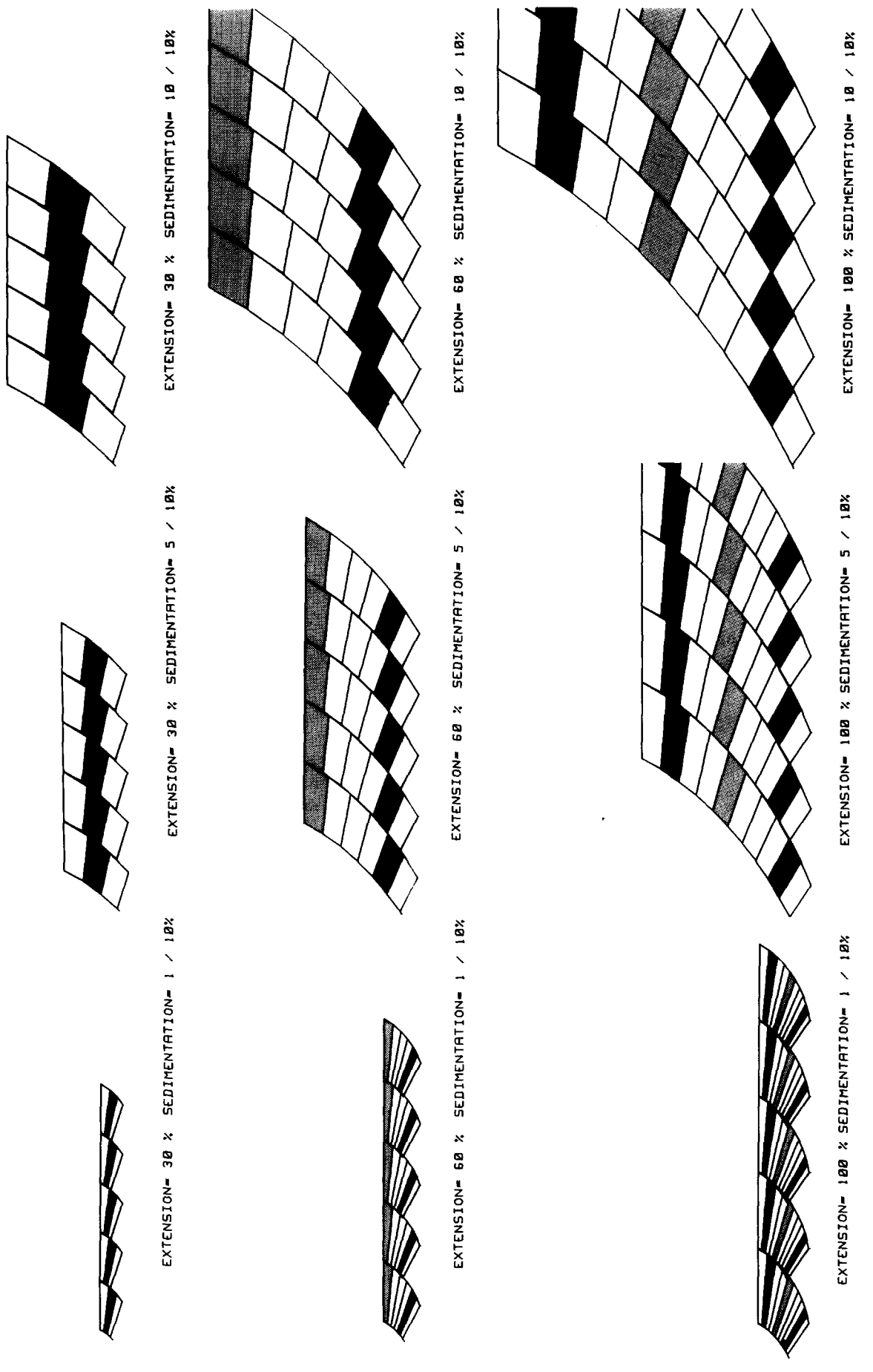

Fig. 4. Results of geometric model of stepwise sedimentation, for three percentages of bulk extension (rows) and three relative rates of sedimentation and extension (columns). Each ornament indicates a stratigraphic level of a given age. See text for interpretation.

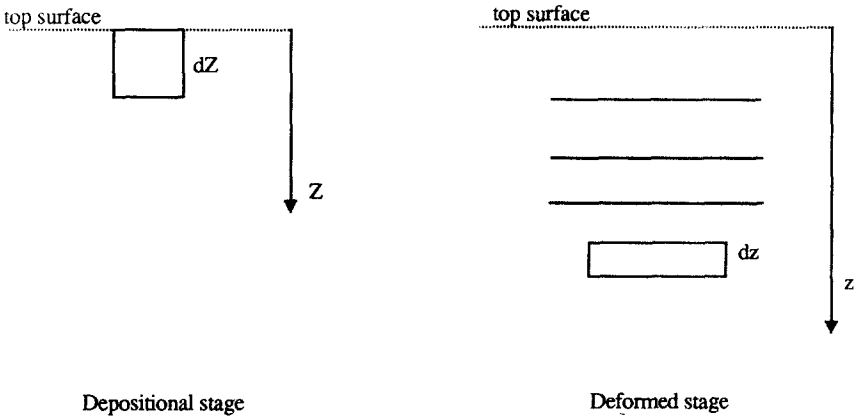

Fig. 5. Geometric model of continuous sedmentation and deformation: material element before deformation (dZ) and after deformation (dz). See text for explanations.

This shows that a given ratio R of sedimentation and strain results in vertical stretch gradients in the material of the same magnitude as R. Because R is negative, λ decreases with depth. Once the stretch gradient is set in the material at the surface, it is not modified by subsequent strain, provided this is spatially uniform. Subsequent strain simply decreases values of λ and of z in the same proportion. This is true whether or not R is constant.

If R is constant, simple integration, together with the boundary condition, $\lambda = 1$ where $z = 0$, yields the linear stretch profile:

$$(\lambda - 1) = Rz. \quad (3)$$

This predicts a maximum stratigraphic depth:

$$z_{max} = -1/R \quad (4)$$

when $\lambda = 0$ at the base. This requires infinite time. In practice, z_{max} is approached asymptotically.

A constant R also yields, from (2), a linear relationship between logarithmic stretch ε and undeformed depth, Z:

$$\varepsilon = RZ. \quad (5)$$

In general, if R is not constant, integration of (2) is not obvious. A safe procedure is to first convert time into undeformed depth by integrating $dZ = S\,dt$, to express R in terms of Z, and then obtain ε by integrating $d\varepsilon = R\,dZ$. Finally, integration of $dz = \lambda\,dZ$ yields z.

Once the stretch profile has been obtained, fault orientation can be computed, assuming a domino-type mechanism for bulk strain. If α is fault dip at depth and α_o is fault dip at the surface, we have (Le Pichon & Sibuet 1981):

$$\sin \alpha_o / \sin \alpha = 1/\lambda. \quad (6)$$

Figure 6 shows computed fault profiles derived from linear stretch profiles. Profile shape depends upon total strain (or time) and upon the value of R. For a given total strain, and by using simple changes in scale, profiles with differing R values can be converted one into the other. Using time integration, we have also computed bedding profiles (Fig. 6).

Results

Both the stepwise and the continuous models reproduce the main structural and stratigraphic features described for the sand models, including (i) listric fault profiles, (ii) bedding tilts increasing with depth, (iii) stratigraphic wedges, (iv) horizontal fault spacing decreasing with depth and (v) offsets increasing with depth.

As well as this, the diagrams show that fault curvature decreases only slightly with depth. This explains the almost complete lack of gaps and overlaps between fault blocks (assumed rigid). In contrast, the geometrical problem of gaps and overlaps—typical of any domino-type interpretation—still exists at the base of the models. In nature, we infer that these can be accommodated in two ways. First, according to many authors (Wernicke & Burchfiel 1982, Gibbs 1984, Brun *et al.* 1985) local internal strain can occur at the base of fault blocks and avoid gaps and overlaps, as in model 1 (Fig. 1). Second, since growth faults usually develop above a layer of evaporites or shales, flowage of this basal layer can accommodate rotation of fault blocks in the upper layers (model 2; Fig. 2) and lead to salt rollers. This process can be observed on seismic sections (e.g. Woodbury *et al.* 1973) and in physical experiments which involve block rotation in brittle–ductile models (Faugère & Brun 1984, Brun *et al.* 1985, Vendeville 1987, Vendeville & Cobbold 1987).

The main contribution of the geometric models is to illustrate the importance of relative rates of sedimentation and strain. Slow sedimentation results in small stratigraphic thicknesses and listric faults with large curvature. Rapid sedimentation results in thicker sequences and faults with smaller curvature. Simply expressed, the relative rate of sedimentation controls the vertical scale in the diagrams. Otherwise, diagrams are geometrically identical for equal total extension.

DISCUSSION

Mechanical models of listric faulting previously

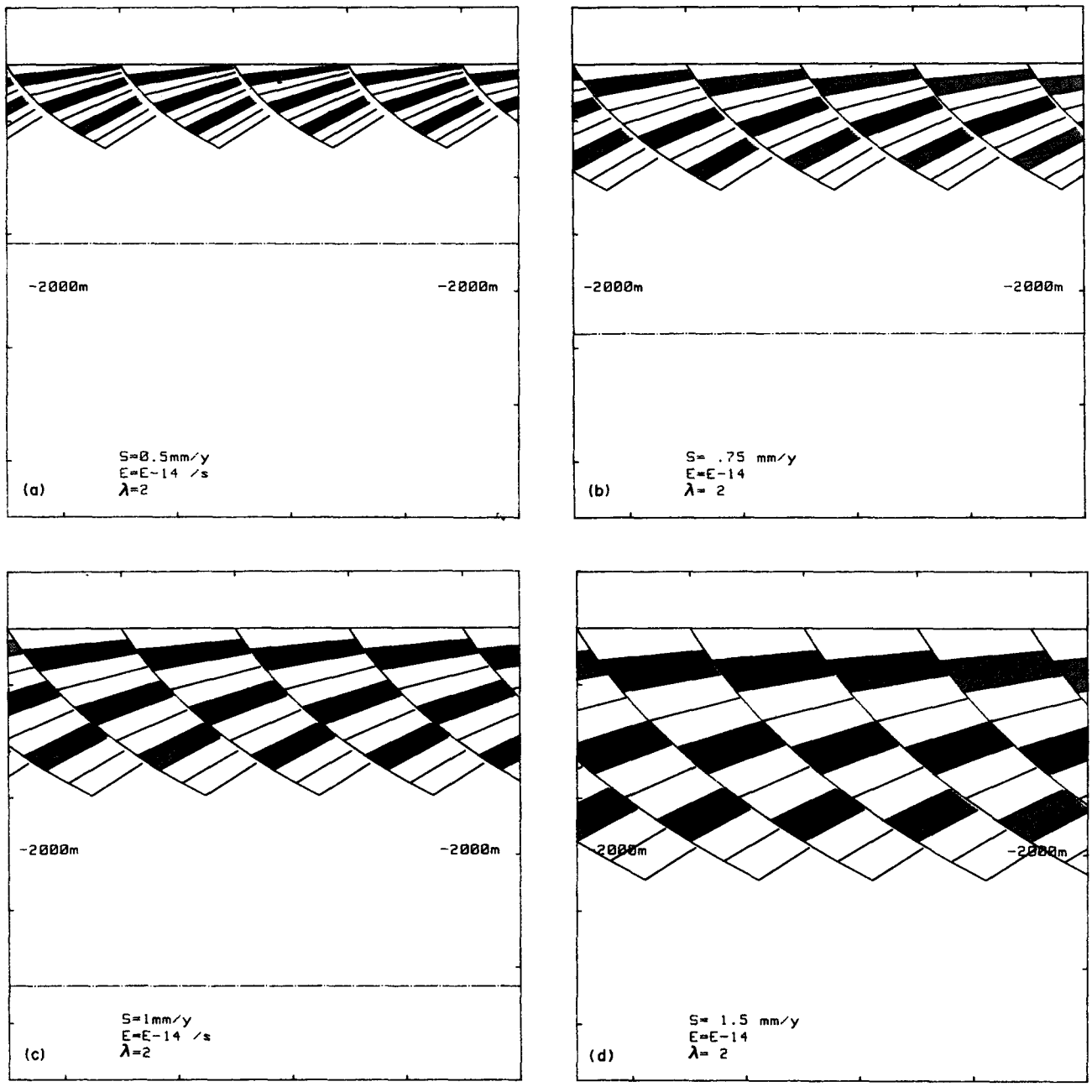

Fig. 6. Results of the geometric model of continuous sedimentation, for a bulk stretch of $\lambda = 2$, a strain rate $\dot{\varepsilon} = 10^{-14}\ s^{-1}$, and four relative rates of sedimentation. Each stratigraphic layer represents a period of 200,000 years. Dashed lines indicate maximum stratigraphic depths, approached after a very large time interval.

developed by Price (1977), Crans *et al.* (1980) and Mandl & Crans (1981) consider that growth faults are listric at initiation because either stress orientation and/or rheology vary with depth. They also assume that growth faults adjust their shapes in order to fit, at any stage of extension, the potential slip plane deduced from stress orientations and rheological conditions. Because such stress values and rheology (including fluid pressure) change with time and deposition of new sediments, the profiles of potential slip planes change as well. To fit them, faults are usually assumed to deform continuously (Mandl & Crans 1981, p. 41).

Although we do not question the fact that faults may initiate in curved form, the present models lead us to believe that at least a part of the finite curvature of growth faults, as observed in the field and in seismic data, may be due to a process of domino-sedimentation.

Supporting evidence comes from other experiments on synsedimentary gravitational gliding (Vendeville 1987, Vendeville & Cobbold 1987). However, seismic sections from the Rhône Delta (Rouchy 1986, Vendeville 1987) and some other growth faulted environments (e.g. Woodbury *et al.* 1973, Edwards 1976, Petrobras 1983a & b, Garfunkel 1984) suggest that domino-sedimentation is not the only cause of fault curvature. For example, the angle between faults and bedding is not strictly conserved, but tends to decrease with depth. We infer that the final fault shape of a growth fault results from a combination of (i) initial curvature, (ii) domino-sedimentation processes, (iii) progressive

compaction and (iv) deformation of the fault plane due to salt or shale diapirism.

What is the range of applicability of the domino-sedimentation model described in this paper?

First, our models suggest that the rates of simultaneous sedimentation and horizontal extension must remain competitive (e.g. $0.1 \text{ mm a}^{-1} < S < 3 \text{ mm a}^{-1}$ for a strain rate $\dot{\varepsilon} = 10^{-14} \text{s}^{-1}$). If R is too low—i.e. the sedimentation rate is high whereas the extension rate is low—fault curvature remains negligible. If R is too high—i.e. the sedimentation rate is low whereas the extension rate is high—sediments only fill the depression between tilted blocks and may not lead to a domino-sedimentation process. Rapid sedimentation and rapid fast extension are known to occurt in deltaic environments, where gravity sliding occurs at shallow depth (a few km) above a detachment horizon (commonly evaporites or overpressured shales). At larger scale, slow sedimentation in continental basins may be competitive with rates of continental extension.

Second, the models assume brittle faulting (Anderson 1951) following a Mohr–Coulomb criterion of failure. This is probably not restrictive and a qualitative application of the domino-sedimentation process remains possible using any mechanism of faulting or localization of deformation into narrow shear zones (brittle–plastic). The only condition is that initial orientations of faults or shear zones are controlled by orientation of the principal stress axes.

Finally the models assume that block rotation results from a mechanism of domino-type. Again, this is not strictly necessary. The interaction between sedimentation, progressive change of fault orientation, and fault propagation upwards may lead to listric growth fault profiles whatever the mechanism responsible for fault reorientation with time and deformation. Other mechanisms can be (i) volume loss associated with progressive compaction or (ii) buckling of the fault plane due to buoyancy effects, such as differential loading due to changes in detrital discharge or salt or shale diapirism below the fault plane.

Acknowledgements—This work was financed jointly by the Compagnie Française des Pétroles (C.F.P.) and the Institut Français du Pétrole (I.F.P.). Special thanks are due to J. C. Chermette (C.F.P.) and to B. Colletta and J. Letouzey (I.F.P.) for their helpful suggestions. We also benefited from useful discussions with P. Szatmari and colleagues at Petrobras, as well as N. Higgs, W. Jamison and S. Serra at Amoco Production Company. We also gratefully acknowledge two anonymous reviewers for suggesting improvements to the initial manuscript. The experiments were done by B. Vendeville ably assisted by B. Goré (University of Rennes). Apparatus was constructed and maintained by CNRS technician J. J. Kermarrec.

REFERENCES

Anadon, P., Cabrera, L., Guimera, J. & Santanach, P. 1985. *Paleogene Strike-slip Deformation and Sedimentation Along the Southeastern Margin of the Ebro Basin* (edited by Biddle, K. T. & Christie-Blick, N.) *Spec. Publs Soc. econ. Palaeont. Miner.* **37**, 303–318.

Anderson, E. M. 1951. *The Dynamics of Faulting and Dyke Formation With Applications to Britain* (2nd edn). Oliver & Boyd, Edinburgh.

Angelier, J. & Colletta, B. 1983. Tension fractures and extensional tectonics. *Nature, Lond.* **301**, 49–51.

Bally, A. W. 1981. Thoughts on the tectonics of folded belts. In: *Thrust and Nappe Tectonics* (edited by McClay, K. R. and Price, N. J.). *Spec. Publs geol. Soc. Lond.* **9**, 13–32.

Bally, A. W., Bernouilly, D., Davis, G. A. & Montadert, L. 1981. Listric normal faults. *Oceanologica Acta, Actes 26ème congrès International de Géologie des marges continentales*, Paris, 7–17 juillet 1980, 87–101.

Beach, A., Bird, T. & Gibbs, A. D. 1987. Extensional tectonics and crustal structure: Deep seismic reflection data from the Northern North Sea Viking Graben. In: *Continental Extensional Tectonics* (edited by Coward, M. P., Dewey, J. F., and Hancock, P. L.). *Spec. Publs geol. Soc. Lond.* **28**, 467–476.

Boillot, G., Montadert, L., Lemoine, M. & Biju-Duval, B. 1984. *Les Marges Continentales Actuelles et Fossiles Autour de la France* (edited by G. Boillot). Masson, Paris.

Bruce, C. H. 1973. Pressured shales and related sediment deformation: mechanisms for development of regional contemporaneous faults. *Bull. Am. Ass. Petrol. Geol.* **57**, 878–886.

Brun, J. P. & Choukroune, P. 1983. Normal faulting, block tilting and decollement in a stretched crust. *Tectonics* **2**, 345–356.

Brun, J. P., Choukroune, P. & Faugère, E. 1985. Les discontinuités significatives de l'amincissement crustal: application aux marges passives. *Bull. Soc. géol. Fr.* **8**, 139–144.

Carver, R. E. 1968. Differential compaction as a cause of regional contemporaneous faults. *Bull. Am. Ass. Petrol. Geol.* **52**, 414–419.

Chenet, P. Y. 1983. Tectonique de rift: l'exemple de la marge continentale de Nord Gascogne. Rapport Institut Français du Pétrole, No. 25542.

Cloos, E. 1968. Experimental analysis of Gulf Coast fracture pattern. *Bull. geol. Soc. Am.* **66**, 241–256.

Crans, W., Mandl, G. & Haremboure, J. 1980. On the theory of growth-faulting, a geometrical delta model based on gravity sliding. *J. Petrol. Geol.* **2**, 265–307.

Delfaud, J. 1977. Sedimentogenesis as linked to the external dynamics of the basins: role of the climate. *Bull. Cent. Recher. Explor.-Prod. ELF-Aquitaine* **1**, 191–216.

Eaton, G. P. 1980. Geological and geophysical characteristics of the Basin and Range province. In: *Continental Tectonics* (edited by Burchfiel, B. C., Oliver, J. E. & Silver, L. T.). Studies in Geophysics, Washington, D.C., 96–113.

Edwards, M. B. 1976. Growth faults in Upper Triassic deltaic sediments, Svaldbard. *Bull. Am. Ass. Petrol. Geol.* **60**, 341–355.

Erxleben, A. W. & Carnahan, G. 1983. Slick Ranch area, Stan County, Texas. In: *Seismic Expression of Structural Styles* (edited by Bally, A. W.). *Am. Ass. Petrol. Geol. Studies in Geology Series* No. 15, **2**, 2.3.1-22–2.3.1-26.

Evamy, B. D., Haremboure, J., Kamerling, P., Knaap, W. A., Molloy, F. A. & Rowland, P. H. 1978. Hydrocarbon habitat of Tertiary Niger delta. *Bull. Am. Ass. Petrol. Geol.* **62**, 1–39.

Ewing, T. E. 1983. Growth faults and salt tectonics in the House diapir province—relative timing and exploration significance. *Trans. Gulf Coast Ass. Geol. Soc. (U.S.A.)* **33**, 83–90.

Ewing, T. E. 1984. Growth faults and salt tectonics. *Oil & Gas J.* **82**, 176–179.

Faugère, E. & Brun, J. P. 1984. Modélisation expérimentale de la distension continentale. *C.r. Acad. Sci. Paris* **299** (II), 365–370.

Garfunkel, Z. 1984. Large-scale submarine slumps and growth faults in the Eastern Mediterranean. *Mar. Geol.* **55**, 305–324.

Gawthorpe, R. L. & Clemmey, H. 1985. Geometry of submarine slides in the Bowland Basin (Dinantian) and their relation to debris flow. *J. geol. Soc. Lond.* **142**, 555–565.

Gibbs, A. D. 1984. Structural evolution of extensional basin margins. *J. geol. Soc. Lond.* **141**, 609–620.

Gibbs, A. D. 1987. Basin development, examples from the United Kingdom and comments on hydrocarbon prospectivity. *Tectonophysics* **133**, 189–198.

Guennoc, P. 1978. Structure et évolution géologique de la pente continentale d'un secteur de l'Atlantique Nord-Est: de la terrasse de Mériadzek à l'éperon de Goban. Unpublished thesis, University of Brest, France.

Hafner, W. 1951. Stress distribution and faulting. *Bull. geol. Soc. Am.* **62**, 373–398.

Horsfield, W. T. 1977. An experimental approach to basement-controlled faulting. In: *Fault Tectonics in NW Europe* (edited by Frost, R. T. C. & Dikkers, A. J.). *Geologie Mijnb.* **56**, 363–370.

Hubbert, M. K. 1937. Theory of scale models as applied to the study of geologic structures. *Bull. geol. Soc. Am.* **48**, 1459–1520.

Hubbert, M. K. 1951. Mechanical basis for certain familiar structures. *Bull. geol. Soc. Am.* **62**, 355–372.

Hubbert, M. K. & Rubey, W. W. 1959. Role of fluid pressure in mechanics of overthrust faulting: I. Mechanics of fluid-filled porous solids and its application to overthrust faulting. *Bull. geol. Soc. Am.* **70**, 115–166.

Jackson, M. P. A. & Galloway, W. E. 1984. Structural and depositional styles of Gulf Coast Tertiary continental margins: application to hydrocarbon exploration. Am. Ass. Petrol Geol., Continuing Education course note series. No. 25.

Jackson, M. P. A. & McKenzie, D. 1983. The geometrical evolution of normal fault systems. *J. Struct. Geol.* **5**, 471–482.

Jones, M. E. & Addis, M. A. 1984. Volume change during sediment diagenesis and the development of growth faults. *Mar. Petrol. Geol.* **1**, 118–122.

Le Pichon, X. & Sibuet, J. C. 1981. Passive margins: a model of formation. *J. geophys. Res.* **86**, 3708–3720.

Lowell, J. F., Genick, G. J., Nelson, T. H. & Tucker, D. M. 1975. Petroleum and plate tectonics of the southern Red Sea. In *Petroleum and Plate Tectonics* (edited by Fisher, A. G. & Judson, S.). Princeton University Press, Princeton, New Jersey, 129–153.

Mandl, G. & Crans, W. 1981. Gravitational gliding in deltas. In:- *Thrust and Nappe Tectonics* (edited by McClay, K. R. and Price, N. J.). *Spec. Publs geol. Soc. Lond.* **9**, 41–54.

Mandl, G., De Jong, L. N. J. & Maltha, A. 1977. Shear zones in granular materials. *Rock Mech.* **9**, 95–144.

Mandl, G. & Fernandez Luque, R. 1970. Fully developed plastic shear flow of granular material. *Géotechnique* **20**, 277–307.

Montadert, L., Roberts, D. G., De Charpal, O. & Guennoc, P. 1979. Rifting and subsidence of the northern continental margin of the Bay of Biscay. Initial Reports DSDP **48**, 1025–1060. U.S. Government Printing Office, Washington, D.C.

Naylor, M. A., Mandl, G. & Sijpesteijn, C. H. K. 1986. Fault geometries in basement-induced wrench faulting under different stress states. *J. Struct. Geol.* **8**, 737–752.

Odé, H. 1960. Faulting as a velocity discontinuity in plastic deformation. In: *Rock Deformation* (edited by Griggs, D. & Handin, J.). *Mem. geol. Soc. Am.* **79**, 293–321.

Petrobras. 1983a. Campos and Espirito basins, offshore Brazil. *Am. Ass. Petrol. Geol. Studies in Geology Series* No. 15, **2**, 2.2.3-51–2.2.3-58.

Petrobras. 1983b. Foz Do Amazonas basin, offshore Brazil. *Am. Ass. Petrol. Geol., Studies in Geology Series* No. 15, **2**, 2.2.3-66–2.2.3-69.

Price, N. J. 1977. Aspects of gravity tectonics and the development of listric faults. *J. geol. Soc. Lond.* **133**, 311–327.

Proffett, J. M. 1977. Cenozoic geology of the Yerington district, Nevada, and implications for the nature of Basin and Range faulting. *Bull. geol. Soc. Am.* **88**, 247–266.

Ramberg, H. 1967. *Gravity, Deformation and the Earth's Crust.* Academic Press, London.

Rettger, R. E. 1935. Experiments on soft rock deformation. *Bull. Am. Ass. Petrol. Geol.* **19**, 271–292.

Rider, M. H. 1978. Growth faults in Carboniferous of Western Ireland. *Bull. Am. Ass. Petrol. Geol.* **62**, 2191–2213.

Rouchy, J. M. 1986. Les évaporites Miocènes de la Méditerranée et de la Mer Rouge et leurs enseignements pour l'interprétation des grandes accumulations évaporitiques d'origine marine. *Bull. Soc. géol. Fr.*, **8**, 511–520.

Roux, W. F. 1979. The development of growth faults structures. *Am. Ass. Petrol. Geol.*, Structural Course Notes.

Shelton, J. W. 1984. Listric normal faults: an illustrated summary. *Bull. Am. Ass. Petrol. Geol.* **68**, 801–815.

Terzaghi, K. 1956. Varieties of submarine slope failures. *Eighth Texas Conference on Soil Mechanics Foundation Engineering*, paper 3.

Truesdell, C. & Toupin, R. 1960. The classical field theories. *Handbuch der Physik* (Encyclopedia of Physics) (edited by Flugge, S.), **3**, 226–793. Springer Verlag, Berlin.

Vendeville, B. 1987. Champs de failles et tectonique en extension: modélisation expérimentale. Unpublished thesis, University of Rennes, France.

Vendeville, B., and Cobbold, P. R. 1987. Synsedimentary gravitational sliding and listric normal growth faults: insights from scaled physical models. *C.r. Acad. Sci. Paris* **305**, 1313–1319.

Vendeville, B., Cobbold, P. R., Davy, P., Burns, J. P. and Choukroune, P. 1987. Physical models of extensional tectonics at various scales: In: *Continental Extensional Tectonics* (edited by Coward, M. P., Dewey, J. F. & Hancock, P. L.). *Spec. Publs geol. Soc. Lond.* **28**, 95–107.

Weber, K. J. & Daukoru, 1976. Petroleum geology of the Niger delta. *Ninth World Petroleum Congress*, Tokyo, **2**, 209–221. Applied Science Publishers, Essex.

Wernicke, B. & Burchfiel, B. C. 1982. Modes of extensional tectonics. *J. Struct. Geol.* **4**, 105–115.

Woodbury, H. O., Murray, I. B., Pickford, P. J., Akers, W. H. 1973. Pliocene depocenters, outer continental shelf, Louisiana and Texas. *Bull. Am. Ass. Petrol. Geol.* **57**, 2428–2439.